Analysis of wall shear stress probes in large amplitude unsteady flows

ZHUOXIONG MAO

Institute of Chemical Metallurgy, Academia Sinica, Beijing 100080, China

and

THOMAS J. HANRATTY

University of Illinois, Urbana, IL 61801, U.S.A.

Abstract—The measurement of the mass transfer rate to flush mounted wall electrodes is a commonly used method to determine the wall shear stress. An analysis for the performance of these probes in the presence of large amplitude unsteady flows is presented. This is accomplished by using numerical solutions of the direct (the variation of the wall shear stress with time is given) and the inverse problem (the variation of mass transfer rate with time is given). For cases in which flow reversal occurs additional information about the flow direction is needed.

1. INTRODUCTION

SMALL electrodes mounted flush to a wall are widely used to measure the wall shear rate in flow systems. (The wall shear stress can then be calculated if the viscosity of the fluid is known.) These electrodes are part of an electrolysis cell in which the other electrode has a much larger area. An electrochemical reaction is carried out on the surface of the test electrode under conditions that the reaction rate is fast enough that the concentration of the reacting species is zero at the surface and the electrochemical process is controlled by the rate of mass transfer, n, to the test electrode. A solution of the mass balance equations for steady flow conditions shows that the measured electric current is proportional to the one-third power of the wall shear rate, s. A thorough review of experimental and theoretical problems related to the use of this technique is given in ref. [1]. This paper extends the range of usefulness by presenting a mathematical analysis for flows which have large amplitude flow variations.

In unsteady flows the time variation of the wall shear stress causes a time variation of the mass transfer rate. If the variation of s is slow enough the one-third power law can still be applied to relate the instantaneous wall shear rate to the instantaneous current. However, in most cases, the inertia of the concentration boundary layer cannot be ignored and the quasi-steady assumption is not valid.

Most of the work on the frequency response of heat or mass transfer probes [2–7] has involved the assumption that the amplitude of the fluctuations is small compared to the time-averaged flow (such as would be the case for 'steady' turbulent flow over a flat surface). In this case a mass transfer variation of

a given frequency is directly related to an s variation of the same frequency. Therefore, if the response of the electrode to sinusoidal fluctuations of different frequencies is known the frequency spectrum of s can be related to the measured frequency spectrum of $n(t)$ by the superposition principle.

Ramaprian and Tu [8] reported on difficulties in interpreting measurements from wall shear stress probes in studies of the influence of imposed flow oscillations of large amplitude. Kaiping [9] presented numerical results on the response of a wall probe to a flow which consists of a steady velocity plus a large amplitude sinusoidal variation. His results show that, as the frequency increases, the departure from quasi-steady behavior becomes more important. This effect is manifested by increases in the amplitude and phase, and a change in the form (both for reversing and non-reversing flows) of the curve representing $n(t)$. Pedley [10] approximated the heat transfer from a hot film probe in reversing shear flows with a combination of a quasi-steady solution and a pure diffusion solution and showed that $n(t)$ deviates considerably from the quasi-steady solution.

This paper is related to that of Kaiping [9] and of Pedley [10] who calculated $n(t)$ for a given $s(t)$. It differs in that it focuses upon the inverse problem of calculating $s(t)$ from a measured $n(t)$. Considerable attention has been given to the problem of inverse heat conduction, as summarized by Beck *et al.* [11]. The presence of a convection term in the mass or heat balance equation for wall probes, however, makes the analysis considerably more difficult. Moreover, when temporally reversing flow happens close to the wall the inverse problem is not unique. Two approaches are considered: in one of these a function for $s(t)$

NOMENCLATURE

A	area of electrode [m^2]
c	concentration [mol m^{-3}]
c_b	bulk concentration [mol m^{-3}]
C	dimensionless concentration
D	molecular diffusivity [m^2 s^{-1}]
F	Faraday's constant
h_x	ratio of consecutive grid spacings in x for electrode
h_y	ratio of consecutive grid spacings in y
h_{xw}	ratio of consecutive grid spacings in x for wake region
I	electric current [A]
L	length of electrode [m]
L^+	dimensionless length of electrode
L_w	dimensionless length of wake region
K	mass transfer coefficient [m s^{-1}]
M	measured modified Nusselt number
n	total mass flux on the electrode [mol m^{-2} s^{-1}]
n'	fluctuation of mass flux
Nu^*	modified Nusselt number, $KL/D(L^{+2}\,Sc)^{-1/3}$
Nu_s^*	modified Nusselt number of quasi-steady solution
n_e	number of electrons transferred in the electrochemical reaction
s	shear rate at the wall [s^{-1}]
$\bar{s}$	time averaged shear rate at the wall
s'	fluctuation of shear rate
S	dimensionless shear rate at the wall, $s/\bar{s}$
$\hat{S}$	amplitude of dimensionless shear rate at the wall
Sc	Schmidt number, ν/D
t	time [s]
U	velocity in the x-direction [m s^{-1}]
V	velocity in the y-direction [m s^{-1}]
x	distance in the streamwise direction [m]
X	dimensionless distance in the streamwise direction, x/L

y	distance normal to the wall [m]
Y	dimensionless distance normal to the wall, $(y^+\,Sc^{1/3})/L^{+1/3}$.

Greek symbols

$\beta_1, \beta_2, \beta_3$	parameters defined in equation (29)
$\Delta X, \Delta Y, \Delta\tau$	steps in the appropriate coordinate directions
$\delta Y_u, \delta Y_d$	half steps in Fig. 1
δ_c^+	dimensionless concentration boundary thickness
δ_c^*	dimensionless concentration boundary thickness defined in equation (23)
ε	small number for convergence or perturbation
τ	dimensionless time, $t^+(Sc^{1/3}\,L^{2/3})^{-1}$
τ_0, τ_1	times of flow reversal starting and ending, respectively
τ_w	wall shear stress [N m^{-2}]
ω^*	dimensionless angular frequency, $2\pi/\tau_p$, where τ_p is the dimensionless time period.

Subscripts

i, j, k	index for the coordinate directions X, Y, τ, respectively
l, r, u, d	left, right, up and down interfaces of the control volume, respectively
L, R, U, D, P	grid points.

Superscripts

0	previous time step or trial value
$\hat{}$	amplitude
$-$	time averaged
$+$	nondimensionalized with wall parameters: friction velocity u^* and kinematic viscosity ν.

with several unknown parameters is assumed. These parameters are selected through an iterative numerical scheme that calculates $n(t)$. The second approach does not estimate the s simultaneously for the whole time domain. Instead, it is assumed that $s(t)$ for $t \leqslant t_k$ is known and that the predicted $n(t)$ for $t \leqslant t_k$ is a good fit to the measurements. Then the wall shear rate is calculated at t_{k+1} from the experimental data on n at t_{k+1} and the knowledge about $s(t)$ for $t \leqslant t_k$.

For cases in which the flow is always moving in the same direction, either of these methods can be used to calculate $s(t)$ from measurements of $n(t)$ obtained with a single probe. However, in cases for which the flow is reversing direction, the solution of the inverse problem requires additional information. The approach taken in this paper is that measurements are available that give the direction of flow at time t, in addition to $n(t)$. One way to obtain this information would be to use a sandwich of two electrodes, as suggested by Son and Hanratty [12], by Py [13], and by Hanratty and Campbell [1].

The results used to test the computational methods were obtained by solving the mass balance equation numerically for sinusoidal wall shear stress variations of different amplitudes and different frequencies. The calculated $n(t)$ relations were then analyzed to obtain the original $s(t)$.

The motivation for the present work is the use of wall transfer probes to study flows with superimposed large amplitude sinusoidal oscillations. Previous

studies by Mao and Hanratty [6] and by Finnicum and Hanratty [14] have been limited to low amplitudes for which a sinusoidal flow oscillation causes a sinusoidal variation in $s(t)$ superimposed on the time-averaged wall shear rate $\bar{s}$. An increase of the amplitude of the flow oscillations eventually is associated with a non-sinusoidal variation of $s(t)$. It has been difficult to determine whether this results from non-linear effects in the turbulence or whether it reflects the probe response.

2. STATEMENT OF THE PROBLEM

A rectangular electrode embedded in the wall with its long side perpendicular to the direction of mean flow is considered as a cathode in an electrochemical cell. The current, I, flowing in the circuit is proportional to the mass flux by the relation

$$n = \frac{I}{Fn_e A}. \tag{1}$$

If the length of the probe in the flow direction is small enough that the thickness of the concentration boundary layer over the electrode is thin compared to the width of the electrode, the concentration field can be described by a two-dimensional mass balance equation

$$\frac{\partial c}{\partial t} + U \frac{\partial c}{\partial x} + V \frac{\partial c}{\partial y} = D \left(\frac{\partial^2 c}{\partial x^2} + \frac{\partial^2 c}{\partial y^2} \right). \tag{2}$$

At high Schmidt number, the thickness of the concentration boundary layer is small enough that the effect of velocities normal to the surface can be neglected and the velocity in the streamwise direction is given by

$$U = s(t)y \tag{3}$$

where $s(t)$ is the time-dependent velocity gradient on the wall. Molecular diffusion in the streamwise direction is normally small compared to streamwise convection in steady flow. Although the diffusion at the two ends of the electrode is not negligible, its influence on the total mass flux to the electrode can still be ignored if the probe is long enough in the flow direction. Ling's numerical solution [15] indicates the error caused by neglecting the streamwise diffusion is less than 5% provided

$$L^{+2} Sc > 200. \tag{4}$$

Here L^+ is the length of the electrode made dimensionless with the friction velocity and the kinematic viscosity. For large amplitude unsteady flows, the velocity gradient can approach zero or pass through zero during a reversing of the flow. Under these conditions it would be suspected that streamwise diffusion cannot be neglected, even if (4) is satisfied. However, an analysis by Kaiping [9] shows that if thermal inertia is important vertical diffusion still dominates over streamwise diffusion and is balanced by thermal

inertia, $\partial c / \partial t$. Therefore, equation (2) is further simplified and written in a dimensionless form as

$$\frac{\partial C}{\partial \tau} + S(\tau) Y \frac{\partial C}{\partial X} = \frac{\partial^2 C}{\partial Y^2} \tag{5}$$

where

$$C = \frac{c}{c_b}, \quad S = \frac{s}{\bar{s}}, \quad X = \frac{x}{L}$$

$$Y = (y^+ Sc^{1/3})/L^{+1/3}, \quad \tau = t^+/(Sc^{1/3} L^{+2/3}). \tag{6}$$

This is solved using the following boundary conditions:

$$C(X, 0, \tau) = 0 \quad \text{for } 0 \leqslant X \leqslant 1$$

$$\left. \frac{\partial C}{\partial Y} \right|_{Y=0} = 0 \quad \text{for } X < 0 \text{ and } X > 1$$

$$\left. \frac{\partial C}{\partial Y} \right|_{Y=\infty} = 0 \quad \text{for all } X$$

$$C = 1 \quad \text{for } X \to -\infty \text{ and } X \to \infty. \tag{7}$$

The first of these boundary conditions arises because of the assumption that the electrochemical system is operated under conditions that the current is controlled by the rate of mass transfer to the test electrode. That is, the reaction rate is fast enough that the concentration of reacting species at the electrode surface is kept at zero.

In solving the direct problem the time-dependent shear rate is assumed to be

$$S = 1 + \hat{S} \cos(\omega^* \tau) \tag{8}$$

and equation (5) is solved to obtain the mass flux on the electrode. A modified Nusselt number Nu^* is defined and calculated from integration of the concentration gradient at the surface along the electrode

$$Nu^* = \frac{KL}{D} (L^{+2} Sc)^{-1/3} = \int_0^1 \left. \frac{\partial C}{\partial Y} \right|_{Y=0} \mathrm{d}X. \tag{9}$$

For steady or quasi-steady flow, the inertia term, $\partial c / \partial t$, in equation (5) is negligible. The solution is then given as

$$Nu_s^* = 0.807 \tag{10}$$

or as

$$\frac{KL}{D} = 0.807 \left(\frac{sL^2}{D} \right)^{1/3}. \tag{11}$$

This is the third power law referenced in Section 1.

3. NUMERICAL METHOD FOR THE DIRECT SOLUTION

For a given time variation of $S(\tau)$, equation (5) is solved numerically, and the modified Nusselt number $Nu^*(\tau)$ is calculated from equation (9). Since the numerical method for solving this direct problem is the main building block for the inverse problem, the
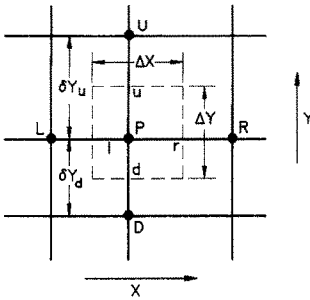
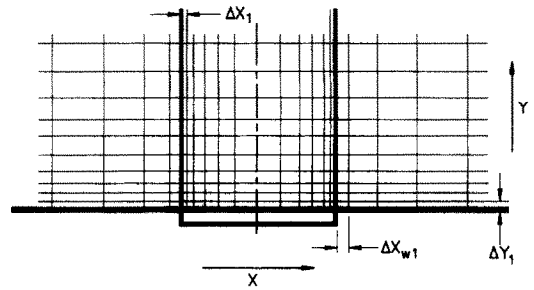FIG. 1. Schematic diagram of the control volume.

FIG. 2. Layout of the computational grids.

numerical scheme should be stable and suitable for both non-reversing and reversing flow. This requires a numerical method different from that used by Kaiping [9]. The control volume method, introduced by Patankar [16], is used to derive a discretized form of equation (5). The advantage of the control volume method is that conservation of mass is exactly satisfied over each volume element, and over the whole domain of calculation, even for the case of a coarse grid. This is extremely important when the equation has non-linear features. Moreover, with the control volume method, variable grid size and discontinuities of the boundary condition can be easily treated.

Each grid point is surrounded by a non-overlapping control volume, as shown in Fig. 1. The concentration between the grid points is assumed to have a piecewise-linear profile. Equation (5) is integrated over each control volume, to give the following discretized form:

$$\frac{C_P - C_P^0}{\Delta \tau} + SY \frac{C_r - C_l}{\Delta X} - \frac{\left(\frac{\partial C}{\partial Y}\right)_u - \left(\frac{\partial C}{\partial Y}\right)_d}{\Delta Y} = 0$$

(12)

where C_r is the concentration on interface r of the control volume and C_l, the concentration on interface l. The convection term in equation (12) is treated with an upwind scheme; i.e.

$$C_r = C_P \atop C_l = C_L \quad \text{if } S > 0 \text{ and } \quad C_r = C_R \atop C_l = C_P \quad \text{if } S < 0. \quad (13)$$

The principle of the upwind scheme is that the concentration at the interface of the control volume is determined by the concentration at the upstream grid point from which molecules are carried by the forced flow to the interface point. The concentration gradients at interfaces u and d are approximated with piecewise-linear profiles

$$\left(\frac{\partial C}{\partial Y}\right)_u = \frac{C_U - C_P}{\delta Y_u} \quad (14)$$

$$\left(\frac{\partial C}{\partial Y}\right)_d = \frac{C_P - C_D}{\delta Y_d}. \quad (15)$$

By substituting equations (13)–(15) into equation

(12), the final form of the finite difference equation is derived as

$$a_p C_P = a_u C_U + a_d C_D + (a_l C_L + a_p^0 C_P^0) \quad \text{for } S > 0$$

(16)

where

$$a_u = \frac{\Delta X}{\delta Y_u}, \quad a_d = \frac{\Delta X}{\delta Y_d}$$

$$a_l = SY\Delta Y, \quad a_p^0 = \frac{\Delta X \Delta Y}{\Delta \tau}$$

$$a_p = a_u + a_d + a_l + a_p^0 \quad (17)$$

and as

$$a_p C_P = a_u C_U + a_d C_D + (a_r C_R + a_p^0 C_P^0) \quad \text{for } S < 0$$

(18)

where

$$a_r = -SY\Delta Y$$

$$a_p = a_u + a_d + a_r + a_p^0 \quad (19)$$

and a_n, a_s and a_p^0 are the same as in equation (17).

If the concentration C_P^0 at the previous time step and the concentration C_L or C_R at the upwind grid point are known, the concentration C_P at the new time can be obtained by solving the set of tridiangular algebraic equations, equation (16) or (18). The coefficients in equations (16) and (18) are all positive, and the coefficient a_p is the sum of the neighboring coefficients. This scheme satisfies the rules described by Patankar [16]. It is a completely implicit scheme, so it is stable for all times.

The layout of the grid points is illustrated in Fig. 2. In the concentration boundary layer the concentration changes dramatically at the leading edge of the electrode and in the region close to the surface of the electrode. In order to resolve this change more accurately, variable grid sizes both in the x-direction and in the y-direction are used

$$\Delta X_i = h_x \Delta X_{i-1} \quad (20)$$

$$\Delta Y_j = h_y \Delta Y_{j-1} \quad (21)$$

where h_x and h_y are greater than 1. In the wake region, the concentration near the trailing edge of the electrode changes rapidly initially and then gradually

approaches the bulk concentration at a large distance away from the trail. Therefore, a variable grid size is also used in this region

$$\Delta X_{w_i} = h_{xw} \Delta X_{w_{i-1}}. \tag{22}$$

The distribution of the grid points is symmetric to the center of the electrode, so that when the flow reverses the grid size is still small enough to resolve the changes at the new leading edge. Therefore, with the present layout of the grid points, both non-reversing and reversing flows can be treated.

For steady flow the thickness of the concentration boundary layer at the end of the electrode can be calculated by defining the outer edge of the concentration boundary as $C = 0.99$

$$\delta_c^* = (\delta_c^+ \, Sc^{1/3})/L^{+\,1/3} = 2.92. \tag{23}$$

In unsteady flow the concentration boundary thickness is varying around its mean value as the shear rate varies. If the shear rate approaches zero, the thickness predicted by equation (23) will approach infinity. However, because of the inertia of the concentration boundary layer this does not occur in the unsteady problem. It has been found that the selection of a computational domain from 0 to 6 in the Y-direction is adequate for the present calculation, in that no difference in the results were noted when an outer boundary of $Y = 4$ was used.

If only non-reversing flow is considered the computational domain in the X-direction is from 0 to 1, which is the space domain of the electrode. However, if there is flow reversal the domain of computation needs to be expanded to cover the wake region since, after a reversal, fluid particles in the wake will be convected to the region above the electrode. The extent of the wake that reaches the electrode after a reversal has been suggested by Kaiping [9] to be

$$L_w = \int_{\tau_0}^{\tau_1} S Y_{max} \, d\tau. \tag{24}$$

This is the maximum distance reached by fluid particles traveling backward during the period of reversing flow. Therefore, the computational domain in the wake region needs to be greater than L_w and to reach a point where the concentration is close to the bulk concentration, as required by boundary condition (7). If the shear rate has the form

$$S = 1 + \hat{S} \cos(\omega^* \tau) \quad \text{and} \quad \hat{S} > 1 \tag{25}$$

then

$$L_w \leqslant \left| \int_{\pi/2}^{3\pi/2} \hat{S} \cos(\omega^* \tau) Y_{max} \frac{d(\omega^* \tau)}{\omega^*} \right|$$

or

$$L_w \leqslant \frac{2 \hat{S} Y_{max}}{\omega^*} = \frac{12 \hat{S}}{\omega^*}. \tag{26}$$

The total wake length, therefore, depends on $\hat{S}$ and

Table 1. Parameters used in the numerical calculation

X	0–1 if $\hat{S} < 1$, $-X_{WK}-(1+X_{WK})$ if $\hat{S} > 1$		
Y	0–6		
ΔX_1	0.001	ΔX_{w1}	0.05
h_x	1.25	h_{xw}	1.75
ΔY_1	0.01	ε	0.001
h_y	1.15		

ω^*. It is selected to be greater than that given by equation (26)

$$X_{WK} = \frac{40 \hat{S}}{\omega^*} \tag{27}$$

in order that the bulk concentration is reached. This selection is conservative, so as to insure that the calculation is not affected by the size of the computation domain. Both the asymptotic solution of Ling [15] and numerical calculations confirm that the boundary condition for $X = \pm \infty$ given in boundary conditions (7) can be accurately represented at X_{WK}. The initial concentration at each grid point was set at 1, except at the surface of the electrode where the concentration is assigned a value of zero. Since the numerical scheme is stable, the selection of the time step was not critical. Sixty-four time steps for each period were chosen, since the use of 128 steps produced the same results.

For each time step, the concentration field at the previous time step and the concentrations at the upstream grid points are known. If the shear rate is positive, the concentration is calculated from the left to the right in Fig. 2 step by step by equation (16). If the shear rate is negative, the calculation is from right to left. The local concentration gradient at the surface of the electrode is calculated as

$$\left. \frac{\partial C}{\partial Y} \right|_{Y=0} = \frac{C(X, Y_2)}{\Delta Y_1} \tag{28}$$

and the total mass flux is calculated by using the trapezoid rule to integrate numerically along the electrode surface.

After calculation over a period is completed, the newly derived $Nu^*(\tau)$ are compared to the values of the previous period. If the difference between the two is greater than a certain value, the newly obtained concentration field is used as the initial condition to continue the calculation for the next period. A stationary solution is usually reached after 3–5 periods. Typical parameters used in the numerical calculations are summarized in Table 1.

4. NUMERICAL METHODS FOR THE INVERSE PROBLEM

4.1. Calculation of S for a whole time domain
A functional form of $S(\tau)$ was assumed as

$$S(\tau) = \beta_1 + \beta_2 \cos(\omega^* \tau + \beta_3). \tag{29}$$

Parameters β_1, β_2 and β_3, are selected so that the

estimated $Nu^*(\tau)$ obtained from a direct numerical solution of the mass balance equation gives the best fit of the measured values of Nu^*, which are represented as $M(\tau)$. In discrete form, let M_k be the measured $Nu^*(\tau)$ and Nu_k^*, the estimated $Nu^*(\tau)$ at given time increments, τ_k. Then, the mean-square error is

$$D = \sum_{k=1}^{r} (M_k - Nu_k^*)^2 \qquad (30)$$

where r is the total number of measurement points. The estimated Nu_k^* depend on parameters β_1, β_2 and β_3. A best fit of Nu_k^* requires

$$\frac{\partial D}{\partial \beta_j} = -2 \sum_{k=1}^{r} (M_k - Nu_k^*) \frac{\partial Nu_k^*}{\partial \beta_j} = 0, \quad j = 1, 2, 3$$

$$(31)$$

where $\partial Nu_k^*/\partial \beta_j$ is the sensitivity coefficient, which indicates how the estimated value Nu^* at time τ_k changes with changes in parameter β_j. If β_j^0 represents a trial value and Nu_k^{*0}, the modified Nusselt number, then the improved value of Nu_k^{*0} can be approximated by a Taylor series expansion around the trial value β_j^0

$$Nu_k^* = Nu_k^{*0} + \sum_{l=1}^{3} (\beta_l - \beta_l^0) \frac{\partial Nu_k^*}{\partial \beta_l}\bigg|_{\beta_l^0}, \quad l = 1, 2, 3.$$

$$(32)$$

After substituting equation (32) into equations (31), the following is derived:

$$\sum_{k=1}^{r} \sum_{l=1}^{3} (\beta_l - \beta_l^0) \left(\frac{\partial Nu_k^*}{\partial \beta_l} \frac{\partial Nu_k^*}{\partial \beta_j} \right)^0$$

$$= \sum_{k=1}^{r} (M_k - Nu_k^{*0}) \left(\frac{\partial Nu_k^{*0}}{\partial \beta_l} \right), \quad j = 1, 2, 3. \quad (33)$$

By solving the above set of equations, an improved set of parameters of β_l is obtained. In order to solve the set of equations (33), Nu_k^{*0} and $(\partial Nu_k^*/\partial \beta_l)^0$ are calculated by solving the direct problem with assumed parameters β_1^0, β_2^0 and β_3^0. The sensitivity coefficients are calculated from equations of the form

$$\left(\frac{\partial Nu_k^*}{\partial \beta_1} \right)^0$$

$$= \frac{Nu_k^*[(1+\varepsilon)\beta_1^0, \beta_2^0, \beta_3^0] - Nu_k^*(\beta_1^0, \beta_2^0, \beta_3^0)}{\varepsilon \beta_1^0} \quad (34)$$

where ε is a small perturbation factor. This requires solving the direct problem four times with four sets of parameters: $[\beta_1^0, \beta_2^0, \beta_3^0]$, $[(1+\varepsilon)\beta_1^0, \beta_2^0, \beta_3^0]$, $[\beta_1^0, (1+\varepsilon)\beta_2^0, \beta_3^0]$, $[\beta_1^0, \beta_2^0, (1+\varepsilon)\beta_3^0]$. The values of Nu_k^*, calculated from equation (32), are compared with the measured values of M_k to decide if another iteration is necessary.

4.2. Calculation of S using sequential estimation

The sequential estimation assumes the variation of the shear rate at time $\tau \leqslant \tau_k$ is known and that the predicted mass flux $Nu^*(\tau)$ fits the data well. Then, the shear rate at time $\tau = \tau_{k+1}$ is estimated from the known experimental data M_{k+1} at $\tau = \tau_{k+1}$.

The mass flux Nu_{k+1}^* at time τ_{k+1} depends on the assumed shear rate S_{k+1} if the concentration field is known at time τ_k. The shear rate at time τ_{k+1} is related to the shear rate at τ_k with

$$S_{k+1}^0 = S_k + \Delta S. \qquad (35)$$

The change of the concentration field from t_k to t_{k+1} is then solved directly to calculate Nu_{k+1}^{*0}. This should match the experimental values of M_{k+1}, given by

$$M_{k+1} = Nu_{k+1}^{*0} + (S_{k+1} - S_{k+1}^0) \frac{\partial Nu^*}{\partial S}\bigg|_{S_{k+1}^0} \quad (36)$$

where S_{k+1} is the correct shear rate at τ_{k+1}. Therefore, the shear rate at time τ_{k+1} is obtained by rearranging the above equation

$$S_{k+1} = S_{k+1}^0 + (M_{k+1} - Nu_{k+1}^{*0}) \bigg/ \frac{\partial Nu^*}{\partial S}\bigg|_{S_{k+1}^0} \quad (37)$$

where the sensitivity coefficient $\partial Nu^*/\partial S|_{S_{k+1}^0}$ is calculated by solving the direct problem

$$\frac{\partial Nu^*}{\partial S}\bigg|_{S_{k+1}^0} = \frac{Nu_{k+1}^*[(1+\varepsilon)S_{k+1}^0] - Nu_{k+1}^*(S_{k+1}^0)}{\varepsilon S_{k+1}^0}.$$

$$(38)$$

The concentration field at τ_{k+1} is recalculated by using the new estimated shear rate S_{k+1} to give a mass flux Nu_{k+1}^* which is closer to the experimental data than Nu_{k+1}^{*0}.

The chief difficulty in using this method is the start, where both the concentration field at τ_0 and the shear rate at τ_1 need to be guessed.

5. RESULTS ON THE DIRECT PROBLEM

Equation (5) has been solved by assuming a sinusoidal variation of the shear rate, i.e. equation (8). Amplitude $\hat{S}$ and frequency ω^* were varied to find their effects on the calculated total mass flux to the electrode. The same values of $\hat{S}$ and ω^* as used by Kaiping were explored in order to compare numerical results.

For an amplitude of 0.5 the shape of the mass flux profile is close to that predicted by quasi-steady state theory. It is noted that an increase in ω^* from 0.5 to 2.0 causes a decrease in the amplitude and a shift in the phase of the sinusoidal function describing the shear rate variation, as predicted by the linear theory presented in ref. [5]. Correction factors, ϕ for the phase and $1/A^2$ for the amplitude, derived from the

Table 2. Correction factors obtained from the inverse method and the linear theory ($\hat{S} = 0.5$)

| | ϕ | | $1/A^2$ | |
ω^*	Linear theory	Inverse method	Linear theory	Inverse method
0.5	$8°$	$8.5°$	~ 1.00	~ 1.00
2.0	$31°$	$33°$	1.25	1.32

inverse method are compared with the ones from the linear theory in Table 2.

For a large value of 0.9 the mass flux profile, shown in Fig. 3, no longer has the sinusoidal shape that would be displayed by the quasi-steady state solution. It is noted that the maximum value is the same for all frequencies and close to that predicted by quasi-steady theory. However, the magnitudes of the minima of the mass flux are strongly influenced by ω^*. The maximum corresponds roughly to the maximum in the shear rate so the convection term dominates the inertia term, $\partial c/\partial t$, in equation (5). On the other hand, the shear rate is small when the mass flux is a minimum, and the inertia is important. It is noted that the distortion of the flux profile increases with increasing ω^*.

When the amplitude of the sinusoidal shear rate function is greater than one, flow reversal occurs at the wall over part of the cycle. Results for amplitudes of 2 and 6.4 are shown in Figs. 4(a) and (b). When the shear rate is negative the mass flux is positive, so the curves characterizing the time variations of the mass flux and the shear rate are quite different. Changes in the frequency have a strong effect. The hump in the mass transfer rate corresponding to the minimum in the shear tends to become smeared as the frequency increases. The phase at which the flow changes direction corresponds roughly to inflection points in the mass transfer profile.

The problem of using mass transfer profiles of the type shown in Figs. 4(a) and (b) to predict shear rate profiles becomes evident. It would be hard to guess that such mass transfer results are caused by a sinusoidally varying shear rate.
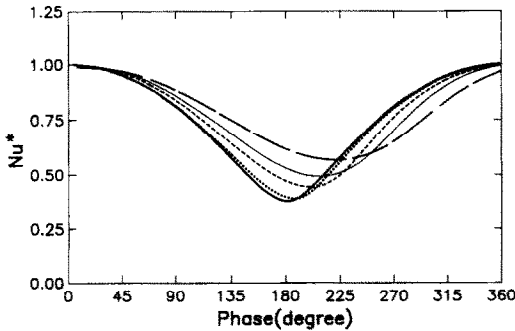
FIG. 3. Numerical calculations of the modified Nusselt number for shear rate: $S = 1 + 0.9 \cos (\omega^*\tau)$; ——, quasi-steady solution; ····, $\omega^* = 0.1$; ----, $\omega^* = 0.5$; ——, $\omega^* = 1.0$; ——, $\omega^* = 2.0$.
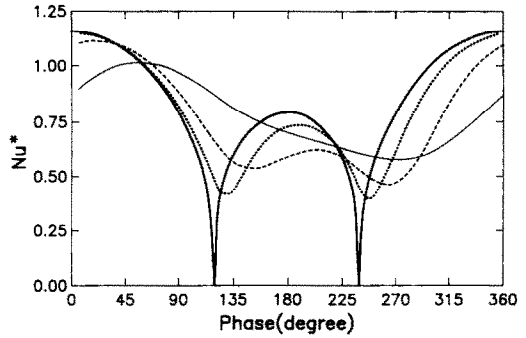

FIG. 4(a). Numerical calculations of the modified Nusselt number for shear rate: $S = 1 + 2.0 \cos (\omega^*\tau)$; ——, quasi-steady solution; ····, $\omega^* = 0.2$; ----, $\omega^* = 1.0$; ——, $\omega^* = 5.0$.
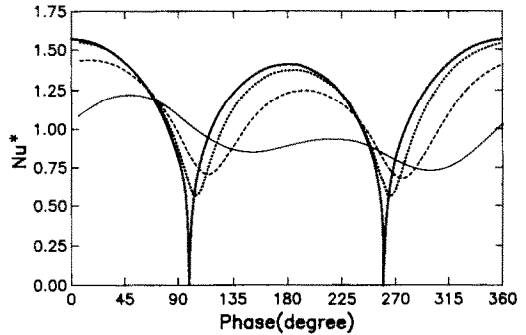

FIG. 4(b). Numerical calculations of the modified Nusselt number for shear rate: $S = 1 + 6.4 \cos (\omega^*\tau)$; ——, quasi-steady solution; ····, $\omega^* = 0.2$; ----, $\omega^* = 1.0$; ——, $\omega^* = 5.0$.

It is to be noted that Figs. 3 and 4 are in good agreement with results calculated by Kaiping [9] with a different numerical algorithm.

6. RESULTS ON THE INVERSE PROBLEM

6.1. Calculation of S for the whole time domain

The mass transfer profiles in Figs. 3 and 4 were used to test the inverse methods outlined in Section 4. For non-reversing flows the whole time method works quite well. For a sinusoidal variation of shear rate, the left-hand side of equation (33) becomes zero, if the estimation is done for the whole period, since the periodic behavior of the function makes the summation of the products of sensitivity coefficients equal to zero. Therefore, the period is broken into four quarters; each quarter is analyzed in sequence. The estimated parameters for each quarter are then averaged. An example of an estimation is given in Table 3. The mass transfer profile analyzed is for $\omega^* = 1.0$

Table 3. An example of whole time domain estimation

	First guess	Final estimation	Input shear rate
β_1	0.8	0.9998	1.000
β_2	0.5	0.9002	0.9000
β_3	$\pi/6$	9.6×10^{-6}	0.0000

FIG. 5. Wall shear rate profiles for the mass fluxes shown in Fig. 3, estimated by the sequential technique.

FIG. 6(a). Wall shear rate profiles for the mass fluxes shown in Fig. 4(a), estimated by the sequential technique.
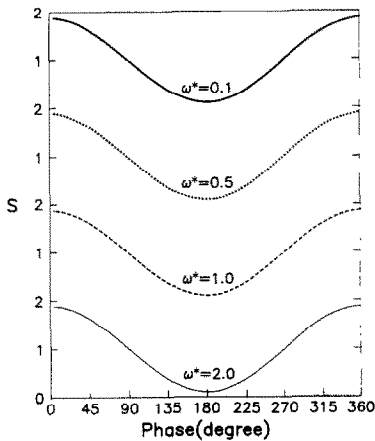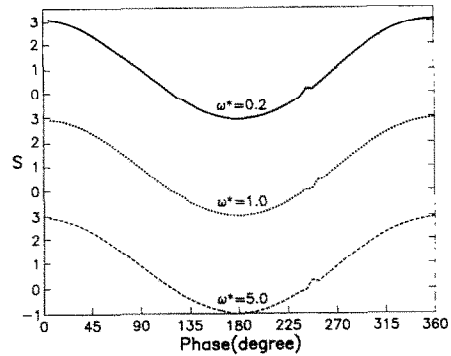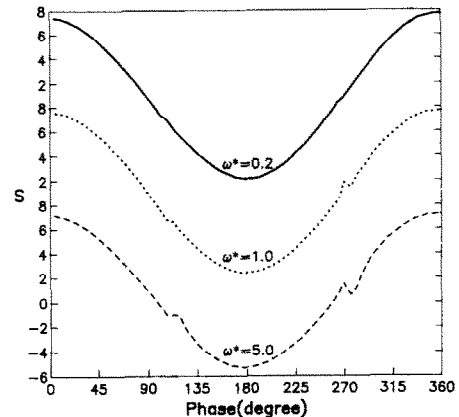

FIG. 6(b). Wall shear rate profiles for the mass fluxes shown in Fig. 4(b), estimated by the sequential technique.

given in Fig. 3. An arbitrary first guess of the parameters is shown in the first column of the table. After several iterations, the estimated parameters, listed in the second column of the table, are close to the values characterizing the input shear rate.

This method was not able to treat problems with flow reversals. The first guess of the shear variation might be so far off from the true one that the predicted reversal points (shear rate changing from positive to negative and from negative to positive) are very different from the true ones. At the estimated turnover points, the numerical calculation changes marching direction and will result in a set of sensitivity coefficients that is completely different from that of the real situation for which the flow has not yet changed direction.

6.2. Sequential estimation of the shear variation

The sequential estimation technique outlined in Section 4.2 was applied to the time variations of the mass flux shown in Fig. 3. The shear rate profiles calculated for the three mass flux profiles (shown in Fig. 5) agree almost exactly with the relation $S = 1 + 0.9 \cos(\omega^* \tau)$ used to generate curves in Fig. 3. This indicates that the method works quite well for non-reversing flows.

The sequential estimation was started at the maximum mass flux and equation (11) was used to estimate a shear rate at the phase angle corresponding to the maximum. This estimated shear rate and the calculated concentration field were used as the conditions at the initial time, τ_0. For the case of a periodic shear rate variation without flow reversal, the calculated shear rate profile does not change after three or four periods and converges to the correct solution.

The shear rate profiles shown in Figs. 6(a) and (b) were calculated with sequential estimation technique from the mass flux profiles for reversing flows shown in Figs. 4(a) and (b). It is to be noted that in this case the direction of flow (in addition to the mass flux profile) was assumed to be known. It is seen in Fig.

6(a) that the estimated shear variations for different frequencies are very close to the correct one. There is only a minor scatter in the points just after flow reversal. For $\hat{S} = 6.4$, as shown in Fig. 6(b), the scatter is larger and the estimation is not so good as for $\hat{S} = 2.0$, in Fig. 6(a). However, considering the large amplitude of the shear rate variations compared to the mean shear rate, the estimation of the shear variation is good.

The estimation of initial conditions, i.e. the shear rate and the concentration field, with the maximum mass flux and the quasi-steady solution is less accurate for profiles with reversing flows. This can be seen in Figs. 4(a) and (b) where the mass fluxes corresponding to the maximum shear rate are seen to deviate considerably from the quasi-steady solution. The consequence of this is that a longer time is required for the solution to converge.

Another problem encountered in solving the inverse problem with flow reversal is the calculation near the point where flow reversal occurs. The actual variations of shear rate and mass flux are continuous, but the estimation is in discrete form. Consequently, the turnover point in the numerical calculation can deviate from the actual one. This discrepancy is probably causing deviations of the estimated shear rate from the real ones after flow reversal. Beck et al. [11] suggested

that the stability of the estimation can be greatly improved if the shear rate at times τ_{k+1}, $\tau_{k+2}, \ldots$, τ_{k+r-1} are assumed equal to the shear rate at time τ_k, and if the measured signals at those time points are used to estimate the shear rate S_k at time τ_k. However, this will not work near points of flow reversal. If the shear rate at the time just before the flow reversal is to be estimated, the assumption that the shear rates at the next several time points equal the shear rate at this time point is obviously bad, since the marching direction in X at those time points stays the same as at the time point before the flow reversal, even though the flow has reversed. As a consequence, the concentration fields and the sensitivity coefficients are miscalculated. Diffusion in the X-direction could be important at the moment flow reversal occurs. Since the present estimation is based on results obtained from the direct solution with no x-diffusion, the deviation near the turnover point cannot be associated with the neglect of this term. However, the effect of x-diffusion on the accuracy of the results for the direct and the inverse problems, especially at the moment of flow reversal, needs to be given further attention. Despite these difficulties the sequential method used in the present work gives a good estimation of the shear variation even for large amplitudes and high frequencies.

7. CONCLUSION

Numerical methods are used to solve the direct and the inverse mass transfer problems for an electrochemical wall probe. The results indicate that the use of the quasi-steady solution to interpret the measured mass transfer rates will cause severe errors in the measurement of wall shear stress for large amplitude unsteady flows. The method outlined in this paper to solve the inverse mass transfer problem provides a possible way to recover the shear stress variation from the measured mass transfer signal. For the cases with flow reversal additional information about flow direction is needed to solve the inverse problem.

REFERENCES

1. T. J. Hanratty and J. A. Campbell, Measurement of wall shear stress. In *Fluid Mechanics Measurements* (Edited by R. J. Goldstein). Hemisphere, Washington, DC (1983).
2. M. J. Lighthill, The responses of laminar skin friction and heat transfer to fluctuations in the stream velocity, *Proc. R. Soc.* **244A**, 1 (1954).
3. B. J. Bellhouse and D. L. Schultz, The determination of fluctuating velocity in air with heated thin film gauges, *J. Fluid Mech.* **32**, 675 (1968).
4. G. Fortuna and T. J. Hanratty, Frequency response of the boundary layer on wall transfer probes, *Int. J. Heat Mass Transfer* **14**, 1499 (1971).
5. Z. Mao and T. J. Hanratty, The use of scalar transport probes to measure wall shear stress in a flow with imposed oscillations, *Exp. Fluids* **3**, 129–135 (1985).
6. Z. Mao and T. J. Hanratty, Studies of the wall shear stress in a turbulent pulsating pipe flow, *J. Fluid Mech.* **170**, 545–564 (1986).
7. A. Ambari, C. Deslouis and B. Tribollet, Frequency response of the mass transfer rate in a modulated flow at electrochemical probes, *Int. J. Heat Mass Transfer* **29**, 35–45 (1986).
8. B. R. Ramaprian and S. W. Tu, Fully developed periodic turbulent pipe flow. Part 2. The detailed structure of the flow, *J. Fluid Mech.* **137**, 59 (1983).
9. P. Kaiping, Unsteady forced convective heat transfer from a hot film in non-reversing and reversing flow, *Int. J. Heat Mass Transfer* **26**, 545–557 (1983).
10. T. J. Pedley, Heat transfer from a hot film in reversing shear flow, *J. Fluid Mech.* **78**, 513–534 (1976).
11. J. V. Beck, B. Blackwell and C. R. St. Clair, Jr., *Inverse Heat Conduction, Ill-posed Problems*. Wiley, New York (1985).
12. J. S. Son and T. J. Hanratty, Velocity gradients at the wall for flow around a cylinder at Reynolds numbers from 5×10^3 to 10^6, *J. Fluid Mech.* **35**, 353–368 (1969).
13. B. Py, Etude tridimensionella de la sous-couche visqueuse dans une veine rectangulaire par des mesures de transfert de matiere en paroi, *Int. J. Heat Mass Transfer* **16**, 129 (1973).
14. D. S. Finnicum and T. J. Hanratty, Influence of imposed flow oscillations on turbulence, *PhysicoChem. Hydrodyn.* **120**, 585–598 (1988).
15. S. C. Ling, Heat transfer from a small isothermal spanwise strip on an insulated boundary, *J. Heat Transfer* **85**, 230 (1963).
16. S. V. Patankar, *Numerical Heat Transfer and Fluid Flow*. McGraw-Hill, New York (1980).

ANALYSE DES SONDES A CISAILLEMENT PARIETAL POUR DES ECOULEMENTS VARIABLES A LARGE AMPLITUDE

Résumé—La mesure du flux de masse par des électrodes en paroi est une méthode utilisée fréquemment pour déterminer le cisaillement pariétal. On présente une analyse des performances de ces sondes en présence d'écoulement variable à large amplitude. Elle est basée sur des solutions numériques du problème direct (variation du cisaillement en fonction du temps) et inverse (variation du transfert de masse en fonction du temps). Pour les cas où il y a inversion de l'écoulement une information supplémentaire sur la direction de l'écoulement est nécessaire.

UNTERSUCHUNGEN GEMESSENER WANDSCHUBSPANNUNGEN IN NICHTSTATIONÄREN STRÖMUNGEN GROSSER AMPLITUDE

Zusammenfassung—Die Messung des Stofftransports hin zu bündig wandintegrierten Elektroden ist eine gebräuchliche Methode für die Bestimmung der Wandschubspannung. Das Verhalten dieser Sensoren bei nichtstationären Strömungen großer Amplitude wird analysiert. Dies wird durch numerische Lösung des direkten (die zeitliche Veränderung der Wandschubspannung ist gegeben) und des inversen Problems (die zeitliche Veränderung des Stoffübergangs ist gegeben) erreicht. In Fällen einer Strömungsumkehr wird zusätzliche Information über die Strömungsrichtung benötigt.

ИССЛЕДОВАНИЕ РАБОТЫ ДАТЧИКОВ НАПРЯЖЕНИЯ СДВИГА НА СТЕНКЕ ПРИ НЕУСТАНОВИВШИХСЯ ТЕЧЕНИЯХ С БОЛЬШОЙ АМПЛИТУДОЙ

Аннотация—Измерение интенсивности массопереноса к установленным заподлицо со стенкой электродам является общепринятым методом определения сдвигового напряжения на стенке. Анализируются рабочие характеристики этих датчиков при неустановившемся течении с большой амплитудой. Используются численные решения для прямой (дается изменение сдвигового напряжения на стенке со временем) и обратной задачи (дается изменение интенсивности массообмена со временем). В случаях с обращением течения необходима дополнительная информация о направжении течения.